JMEMS Letters

A 2-DOF Electrostatically Actuated MEMS Nanopositioner for On-Chip AFM

A. G. Fowler, A. N. Laskovski, A. C. Hammond, and S. O. R. Moheimani

***Abstract*—A new 2-DOF microelectromechanical systems (MEMS)-based parallel kinematic nanopositioner with electrostatic actuation is presented. The device has been designed, fabricated, and implemented using the silicon-on-insulator-based MEMSCAP SOIMUMPs process. Experimental characterization shows that in-plane displacements in excess of 15 μm are achievable and that the first resonant mode along each axis is located at approximately 820 Hz. The nanopositioner's use in a practical application is demonstrated, with the device being used as the scanning stage during an atomic force microscope scan. [2011-0372]**

***Index Terms*—Atomic force microscopy, electrostatic actuators, microelectromechanical systems (MEMS), nanopositioning.**

I. Introduction

Nanopositioners have seen wide use in a range of microscale applications, including scanning tunneling microscopy [1], atomic force microscopy [2], and ultrahigh-density probe storage systems [3]–[5]. This letter presents a new microelectromechanical systems (MEMS)-based nanopositioner that is designed for use in atomic force microscopy, wherein the scan table is made to track a raster pattern in the x and y planes while a microcantilever conducts measurements in the z-direction.

Atomic force microscopes (AFMs) operate by running a sharp tip over a sample in a raster pattern, such that a 3-D image is obtained based on the z-axis deflection and in-plane position of the tip. Typically, a laser beam is shone on the end of the cantilever, with the deflection of the reflected beam indicating the height of the cantilever and, therefore, the topography of the sample.

The nanopositioner reported in this letter uses electrostatic comb drives to actuate the stage. While thermal and electrostatic actuators are both commonly used in MEMS-based nanopositioner designs and are both straightforward to integrate into a fabricated device, previous nanopositioners that use thermal actuators have been shown to have relatively low operating bandwidths of around 100 Hz [6]–[8]. As the scan speed of an AFM is limited by the operating bandwidth of the nanopositioner [9], the typically higher operating bandwidth of electrostatic-based systems is preferred. It has been demonstrated that high AFM scan rates are of particular importance in the imaging of various biological processes, with a frame capture time of 80 ms being sufficient to analyze the motions of certain proteins [10]. Additionally, in a thermally actuated nanopositioner, there is the potential for the conduction of heat from the actuators to the stage. This is undesirable in an AFM application as this thermal energy may potentially damage a scan sample placed on the stage. Furthermore, the use of electrostatic actuators allows a standardized silicon-on-insulator (SOI)-based MEMS fabrication process to be used, avoiding the more specialized steps involved in fabricating other MEMS-based mechanisms such as electromagnetic or piezoelectric actuators.

While the design does not include a dedicated displacement sensing mechanism, the device is designed such that the position of the stage can be estimated from the actuating voltage with a high degree of confidence. The mechanical layout of the nanopositioner has been designed such that unwanted vibration modes are shifted as much as possible to frequencies far from the operating frequencies.

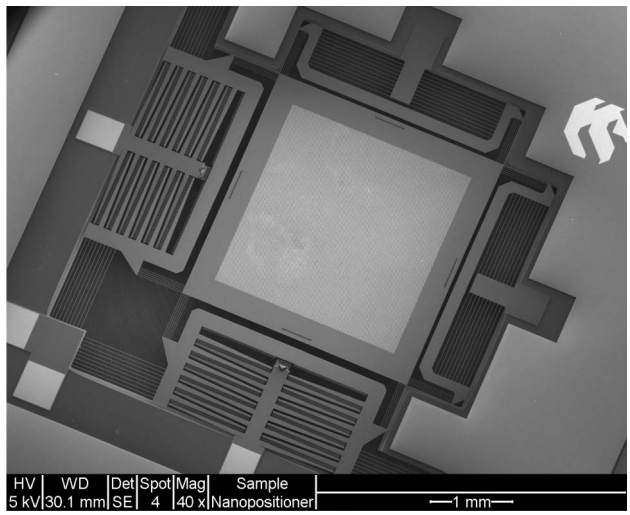

Fig. 1. SEM image of fabricated nanopositioner.

II. Nanopositioner Design and Fabrication

The nanopositioner design consists of a central positioning stage, actuating combs, connecting springs, and the substrate layer, as shown in the scanning electron microscope (SEM) image in Fig. 1. Two comb-drive actuators are positioned at adjacent edges of the device in a unidirectional pull configuration to actuate the stage in the x- and y-directions. To maximize the force generated by the comb structures, both the comb finger width and the distance between comb fingers were set to 2 μm, which is the minimum dimension allowed by the fabrication process. The actuators are then connected to the substrate via beam springs that are oriented perpendicular to the direction of the actuator movement.

The central positioning stage (the scan table) is a solid structure 3 mm $\times$ 3 mm in size and is connected to the electrostatic actuators using beam springs which are oriented parallel to the direction of actuation of the comb.

For accurate positioning of the scan table, it is desirable to have a high stiffness in the out-of-plane (z) direction. This is facilitated by designing the beam springs to be as thin as practical to maximize the out-of-plane spring constant for a given in-plane stiffness. Accordingly, the widths of the beam springs in the design are 3.5 μm, with multiple beams being placed in parallel to achieve the desired in-plane spring constants. The stiffness of the device in the x and y planes is chosen such that the displacement due to the maximum applied voltage is equal to the desired stroke of the nanopositioner.

Manuscript received December 21, 2011; revised March 7, 2012; accepted March 16, 2012. Date of publication April 11, 2012; date of current version July 27, 2012. This work was supported by the Australian Research Council. Subject Editor O. Solgaard.

The authors are with the School of Electrical Engineering and Computer Science, The University of Newcastle Australia, Callaghan, N.S.W. 2308, Australia (e-mail: Reza.Moheimani@newcastle.edu.au).

Color versions of one or more of the figures in this paper are available online at http://ieeexplore.ieee.org.

Digital Object Identifier 10.1109/JMEMS.2012.2191940

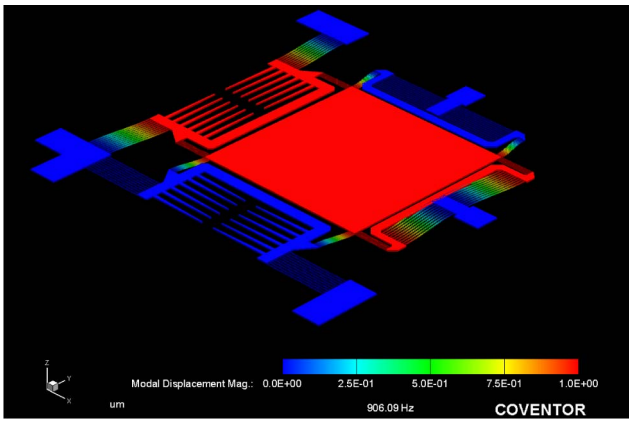

Fig. 2. CoventorWare modal analysis showing the first in-plane resonant mode of nanopositioner.

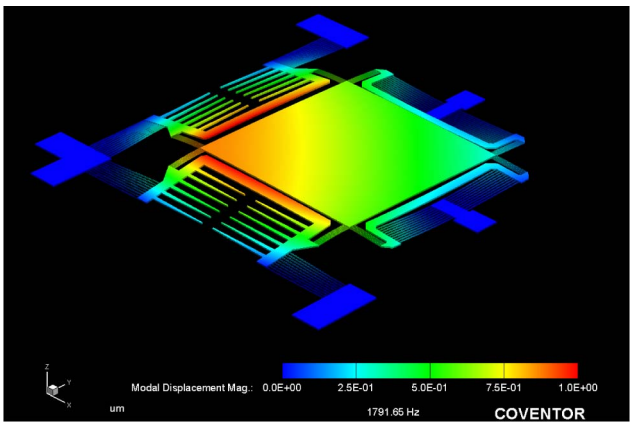

Fig. 3. CoventorWare modal analysis showing higher order resonant mode of nanopositioner.

A large number of electrostatic combs are included within the design to provide a relatively large actuating force. This allows the chosen in-plane spring constants to be similarly high for the desired stroke, increasing the frequency of the first resonant mode of the device.

To prevent rotational oscillations of the stage within the plane, a high degree of torsional rigidity is required about the z-axis. This is aided by concentrating the connecting springs as close to the corners of the stage as possible, which has the effect of reducing the stage's moment of inertia. By using a layout that features many thin beam flexures, the stability of the nanopositioner is increased.

As part of the design process, a finite-element model of the nanopositioner was created using the MEMS design software package CoventorWare. A modal analysis performed on this model indicates that the first in-plane resonant mode along both the x- and y-axes is located at approximately 906 Hz, as shown in Fig. 2. The modal analysis also indicates the presence of a torsional mode at 1792 Hz, as shown in Fig. 3.

The nanopositioner was fabricated using MEMSCAP's SOIMUMPs SOI micromachining process [11]. The main structural features of the device, including the positioning stage, beam springs, and comb-drive actuators, are fabricated from 25-μm-thick doped silicon. This silicon layer is released by a deep-reactive-ion-etching silicon etch that is used to remove the substrate layer from selected areas of the die.

III. Characterization

The in-plane behavior of the nanopositioner was characterized using a Polytec MSA-400 Micro System Analyzer, which uses stroboscopic video microscopy to allow the measurement of in-plane motions. Fig. 4 shows the measured static displacement of the stage versus actuation voltage along both axes. At a maximum applied voltage of 45 V, the obtained displacements were 16 and 15.1 μm along the x- and y-axes, respectively. The frequency response of the nanopositioner along both axes was also analyzed and is shown in Fig. 5, with the experimental data showing that the first resonant modes along the x- and y-axes are located at 816 and 820 Hz, respectively. These experimental results compare favorably with the results of the modal analysis performed via the CoventorWare simulation.

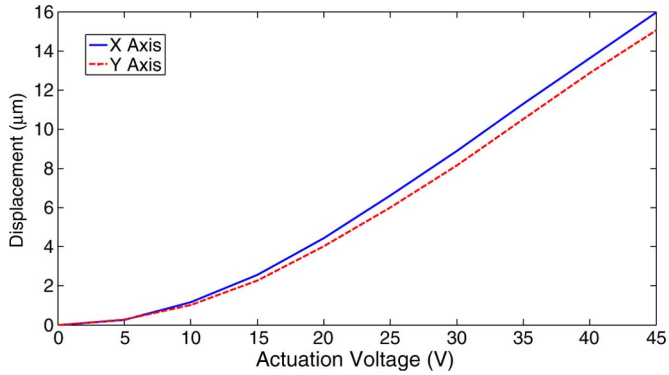

Fig. 4. Displacement versus actuation voltage.

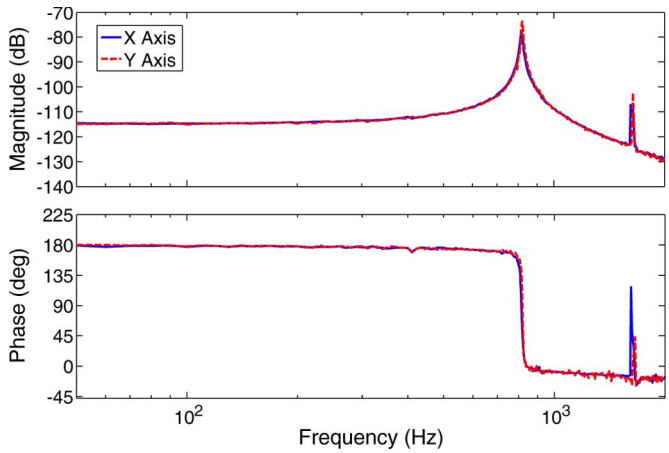

Fig. 5. Frequency response.

The obtained frequency response also shows a higher order resonant mode that is present in both axes at approximately 1.6 kHz, which is close to the simulated resonant mode at 1.792 kHz. Further analysis of the time-domain response of the nanopositioner at this frequency shows highly nonlinear in-plane behavior, with the response of the stage being amplitude dependent and containing harmonics of the exciting signal.

IV. AFM Scan

The nanopositioner was used as the scanning stage of a commercial AFM (NTMDT-NTEGRA), and an open-loop scan was performed in tapping mode. For this purpose, the device's scan table was designed with a repeated array of cylindrical gold features 520 nm high, 3 μm in diameter, and spaced 6 μm apart, as shown in Fig. 6. The resulting image from the AFM scan is shown in Fig. 7.

In the next iteration of this design, a sample would be placed on the stage in lieu of the integrated gold features. This may require a modification of the stage such that it is able to support the added mass and that the bandwidth of the device is not significantly reduced.

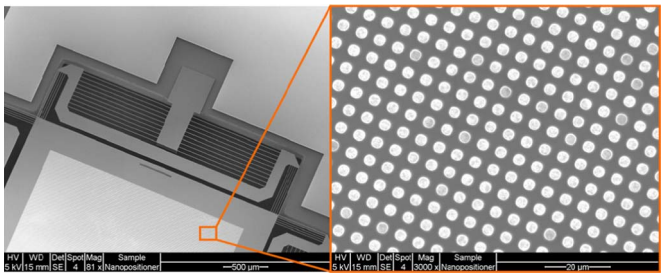

Fig. 6. SEM image of gold features on nanopositioner stage.

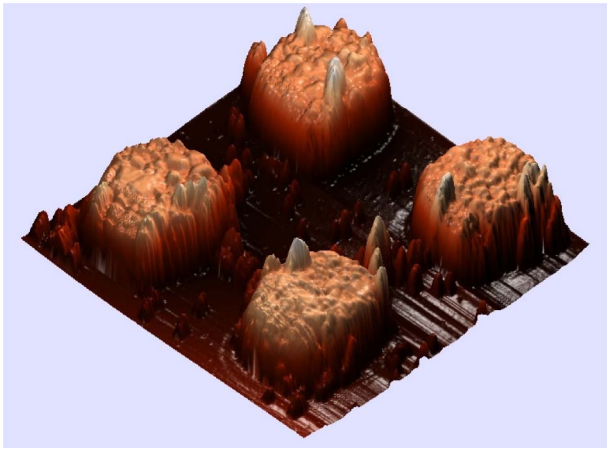

Fig. 7. AFM image of the features on the nanopositioner stage. The image was obtained in tapping mode.

V. Conclusion

These investigations establish the capability of this device to function as the nanopositioning stage of a miniaturized AFM. In addition to offering a smaller footprint compared with existing macroscale stages, this MEMS-based nanopositioner offers low power consumption and a large scan range combined with a relatively high operational bandwidth and uses a standardized MEMS fabrication process for potentially low-cost manufacturing. This design has opened the scope for the development of feedback controllers and high-accuracy low-frequency sensing interface circuitry. These aspects are currently being investigated based on this device, with the view to realize high-speed atomic force microscopy on a chip.

Acknowledgment

The authors would like to thank Dr. Y. Yong for her assistance in generating the atomic force microscope image and the University of Newcastle's Electron Microscope and X-Ray Unit for the access to the scanning electron microscope.

References

[1] G. Binnig and H. Rohrer, "The scanning tunneling microscope," *Sci. Amer.*, vol. 253, pp. 50–56, 1986.
[2] G. Binnig, C. Quate, and C. Gerber, "Atomic force microscope," *Phys. Rev. Lett.*, vol. 56, no. 9, pp. 930–933, Mar. 1986.
[3] N. B. Hubbard, M. L. Culpepper, and L. L. Howell, "Actuators for micropositioners and nanopositioners," *Appl. Mech. Rev.*, vol. 59, no. 6, pp. 324–334, Nov. 2006.
[4] A. Pantazi, M. A. Lantz, G. Cherubini, H. Pozidis, and E. Eleftheriou, "A servomechanism for a micro-electro-mechanical-system-based scanning-probe data storage device," *Nanotechnology*, vol. 15, no. 10, pp. S612–S621, Oct. 2004.
[5] M. A. Lantz, H. E. Rothuizen, U. Drechsler, W. Häberle, and M. Despont, "A vibration resistant nanopositioner for mobile parallel-probe storage applications," *J. Microelectromech. Syst.*, vol. 16, no. 1, pp. 130–139, Feb. 2007.
[6] J. J. Gorman, Y.-S. Kim, and N. G. Dagalakis, "Control of MEMS nanopositioners with nano-scale resolution," in *Proc. ASME Int. Mech. Eng. Congr. Expo*, Chicago, IL, 2006, pp. 151–159.
[7] Y. Zhu, A. Bazaei, S. O. R. Moheimani, and Y. R. Yuce, "Design, modeling, and control of a micromachined nanopositioner with integrated electrothermal actuation and sensing," *J. Microelectromech. Syst.*, vol. 20, no. 3, pp. 711–719, Jun. 2011.
[8] C. Guan and Y. Zhu, "An electrothermal microactuator with Z-shaped beams," *J. Micromech. Microeng.*, vol. 20, no. 8, p. 085014, Aug. 2010.
[9] I. A. Mahmood, S. O. R. Moheimani, and B. Bhikkaji, "A new scanning method for fast atomic force microscopy," *IEEE Trans. Nanotechnol.*, vol. 10, no. 2, pp. 203–216, Mar. 2011.
[10] T. Uchihashi, R. Iino, T. Ando, and H. Noji, "High-speed atomic force microscopy reveals rotary catalysis of rotorless F_1-ATPase," *Science*, vol. 333, no. 6043, pp. 755–758, Aug. 2011.
[11] A. Cowen, G. Hames, D. Monk, S. Wilcenski, and B. Hardy, *SOIMUMPs Design Handbook (Revision 8.0.)*. [Online]. Available: http://www.memscap.com